Acta Crystallographica Section D
Biological Crystallography
ISSN 0907-4449

Preliminary analysis of crystals of panicum mosaic virus (PMV) by X-ray diffraction and atomic force microscopy

Debora L. Makino, Steven B. Larson and Alexander McPherson*

University of California at Irvine, Department of Molecular Biology and Biochemistry, 560 Steinhaus Hall, Irvine, CA 92697-3900, USA

Correspondence e-mail: amcphers@uci.edu

Received 20 September 2004
Accepted 24 November 2004

Panicum mosaic virus (PMV), a spherical virus of diameter about 300 Å, has been crystallized in a form suitable for high-resolution structural analysis. The crystals were grown from 15% PEG 400 at room temperature and could be flash-frozen directly from their mother liquor. The crystals diffracted to beyond 2.7 Å resolution. A data set was collected at 100 K to an effective resolution of 3.2 Å [Weiss (2001), *J. Appl. Cryst.* **34**, 130–135]. The crystals belonged to space group $P2_1$, with unit-cell parameters $a = 411.7$, $b = 403.9$, $c = 412.5$ Å, $\beta = 89.7^\circ$. Self-rotation functions and molecular replacement with tobacco necrosis virus as the probe model yielded tentative positions and orientations for the two entire virus particles comprising the asymmetric unit and implied a pseudo-face-centered cubic packing arrangement. Investigation of lightly glutaraldehyde-fixed crystals in water using atomic force microscopy confirms the packing arrangement given by the molecular-replacement result. The images also show that contaminating virions of the satellite virus to PMV, known as satellite panicum mosaic virus (SPMV), can be incorporated into the PMV crystals by insertion into the interstices between PMV virions in the lattice. This is the first observation of such a phenomenon in macromolecular crystals.

1. Introduction

Panicum mosaic virus (PMV) is a non-enveloped spherical virus that infects plants of the Gramineae family (International Committee on Taxonomy of Viruses; ICTVdB). PMV belongs to the *Panicovirus* genus of the *Tombusviridae* family. The capsid is 30 nm in diameter and is assumed to be a $T = 3$ icosahedral particle and therefore to be composed of 180 protein subunits of identical sequence of approximate molecular weight 26 kDa (Turina *et al.*, 1998). They encapsidate monopartite positive-sense single-stranded RNA molecules 4326 nucleotides in length (Turina *et al.*, 1998).

A unique feature of PMV is that it is one of only four known plant viruses (Ban *et al.*, 1995) that is frequently accompanied in the wild by a satellite virus. The satellite is called satellite panicum mosaic virus (SPMV) and is a $T = 1$ icosahedral particle that is serologically unrelated to its helper virus PMV. Co-infection of pearl millet, the host plant, with PMV and SPMV increases the titer of PMV above its normal level (Scholthof, 1999). The structure of SPMV has previously been solved in this laboratory and refined to 1.9 Å resolution (Ban & McPherson, 1995).

The X-ray structures of four viruses from the *Tombusviridae* family have been reported (http://mmtsb.scripps.edu/viper/). Of those, tobacco necrosis virus (TNV), which is serologically related to TNV strain A (Oda *et al.*, 2000), shows

the highest amino-acid sequence identity to PMV (Turina *et al.*, 1998) at only about 22.6%. Interestingly, the relationship between TNV and its satellite tobacco necrosis virus is analogous to that between PMV and SPMV (Buzen *et al.*, 1984). Because of our continuing interest in the PMV/SPMV relationship, we initiated this effort to determine the crystallographic structure of the helper virus PMV.

2. Materials and methods

2.1. Sample preparation

PMV was prepared from PMV/SPMV co-infected pearl millet leaves, which were grown from seeds of strains German R and Sun Up in a temperature-controlled greenhouse. The virus innoculum for PMV/SPMV was provided to us by Dr Karen Sholthof of Texas A&M University (Scholthof, 1999). Purification steps were as described by Buzen *et al.* (1984), except that PEG 6000 was substituted for PEG 8000 and high-speed centrifugation was replaced by an overnight incubation with 6% PEG 8000 at 277 K followed by 8000*g* centrifugation for 15 min. The PMV-containing pellet was resuspended in 0.05 *M* sodium phosphate pH 6.0 and the last step was repeated. From 100 g of millet leaves, approximately 15 mg PMV was obtained. The virus was concentrated when appropriate using Centriplus YM-100 spin concentrators (Millipore Co., Bedford, MA, USA) with 100 000 Da molecular-weight cutoff and stored at 193 K.

2.2. Crystallization

Over the past ten years, we have made numerous attempts to crystallize PMV and many crystals were grown under a wide variety of conditions. Some of these were quite large and had dimensions of 1 mm or greater. In no case, however, did we obtain from any of them ordered diffraction patterns or patterns that extended to beyond about 15 Å Bragg spacing. This was true at 295 K, so no effort to freeze any of these crystals was attempted.

Ultimately, we focused our attention on preparing and crystallizing PMV entirely under low-pH conditions. The basis for this decision is the observation that for many $T = 3$ icosahedral plant viruses (Kaper, 1975) particle swelling and consequent structural heterogeneity occurs under neutral or alkaline conditions. Using PMV prepared at pH 6.0, we began optimization from crystals grown from condition No. 49 of the Low Ionic Strength Screen (Hampton Research, Aliso Viejo, CA, USA) at 277 K. This solution contains 0.05 *M* sodium acetate pH 4.0 and 30% PEG 400. Vapor diffusion using sitting drops was employed. Generally, the reservoirs were 0.6 ml and the protein drops initially 10 µl consisting of equal volumes of the reservoir solution and a 5 mg ml^{-1} virus stock solution.

Optimization screens over the pH range 2.6–5.5 were performed at room temperature (291 K) and 277 K and other precipitating agents were explored. However, only PEG 400 yielded encouraging results. The buffer concentration, which appeared to be a sensitive parameter, was also varied from 0.05 to 0.20 *M*. In the end, the crystals used for X-ray data collection were obtained after five months at 291 K with the reservoir solution containing 0.1 *M* citric acid pH 5.0–5.5 and 30% PEG 400. In these experiments, however, the initial concentration of the PEG 400 in the virus drop varied from 7.5 to 10%. The initial virus concentration was 5 mg ml^{-1}. PMV crystals presenting different habits, but with the same unit-cell parameters, are shown in Fig. 1.

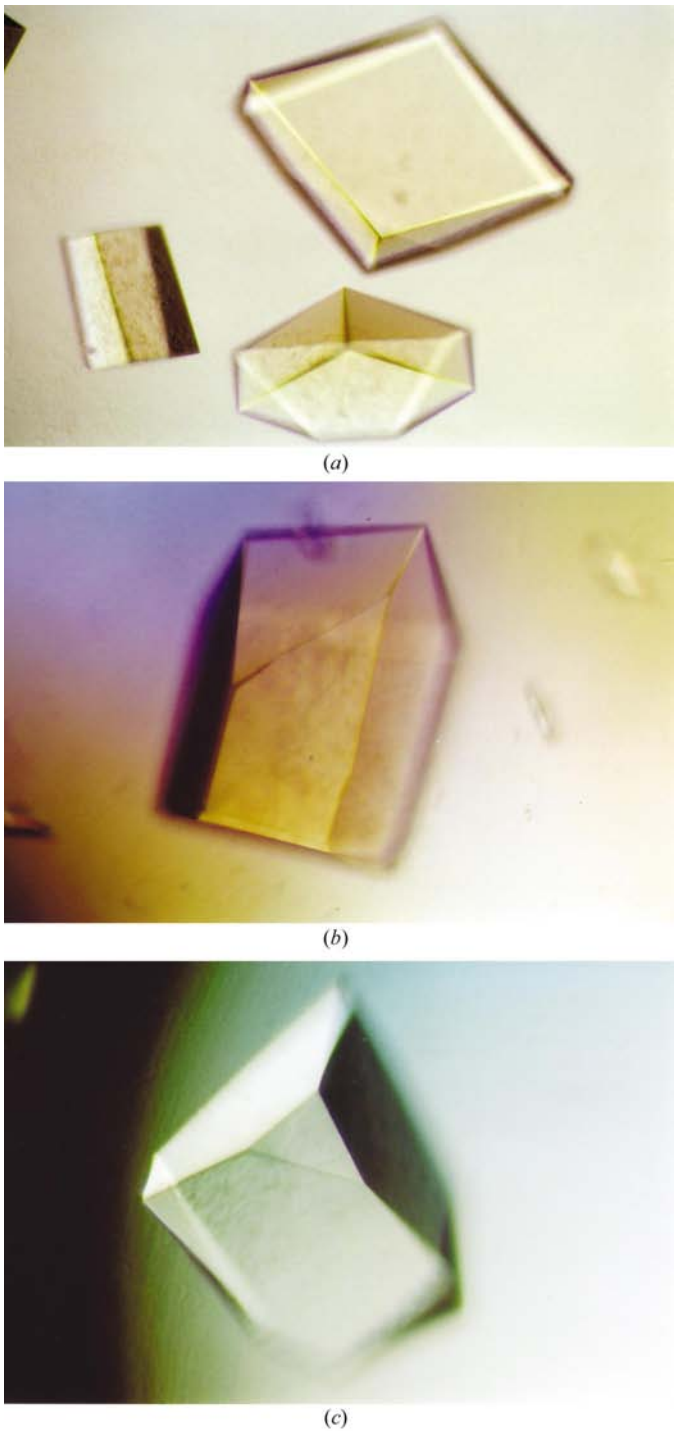

Figure 1
PMV crystals grown in PEG 400 at 291 K by the sitting-drop vapor-diffusion technique: (*a*) pH 4.5, (*b*) pH 5.5, (*c*) pH 5.0.

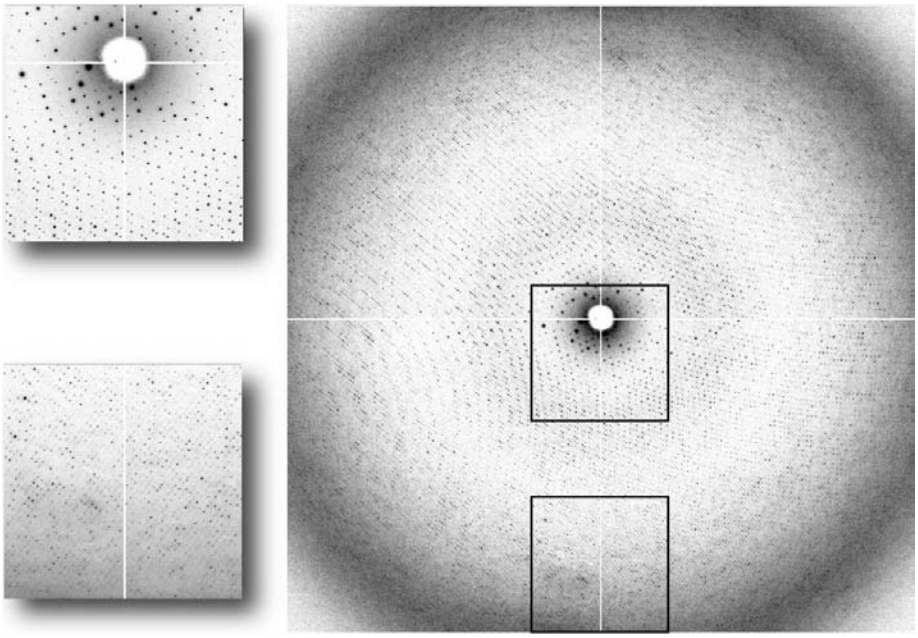

Figure 2
Diffraction image taken from a cryocooled PMV crystal grown in PEG 400 at pH 5.5. The crystal was exposed to 1 Å wavelength radiation at ALS beamline 5.0.2 for 20 s with a 0.5° oscillation angle. Details of the diffraction pattern near the beam center and at the bottom edge are also shown. The resolution limit at the edge is 3.73 Å and that at the corner of the image is 2.71 Å.

2.3. Data collection and data processing

PMV crystals taken directly from their mother liquor were flash-frozen in the cryostream without further treatment and X-ray diffraction data were collected on beamline 5.0.2 at the Advanced Light Source (ALS) of the Lawrence Berkeley National Laboratory. 942 images of 0.5° oscillation angle and exposure time 20 s were recorded from a single frozen crystal using 1.000 Å wavelength X-rays. This crystal was grown in 10% PEG 400 pH 5.5, as described, and shows a similar crystal habit to that in Fig. 1(*b*). To obtain separation of reflections and the highest possible resolution on the 2 × 2 CCD detector, beam divergence was lowered 2.7-fold (horizontal gap of 10 000) and the detector distance was set to 380 mm. A sample image from the data set is shown in Fig. 2. Data processing was carried out using *d*TREK* (Pflu-

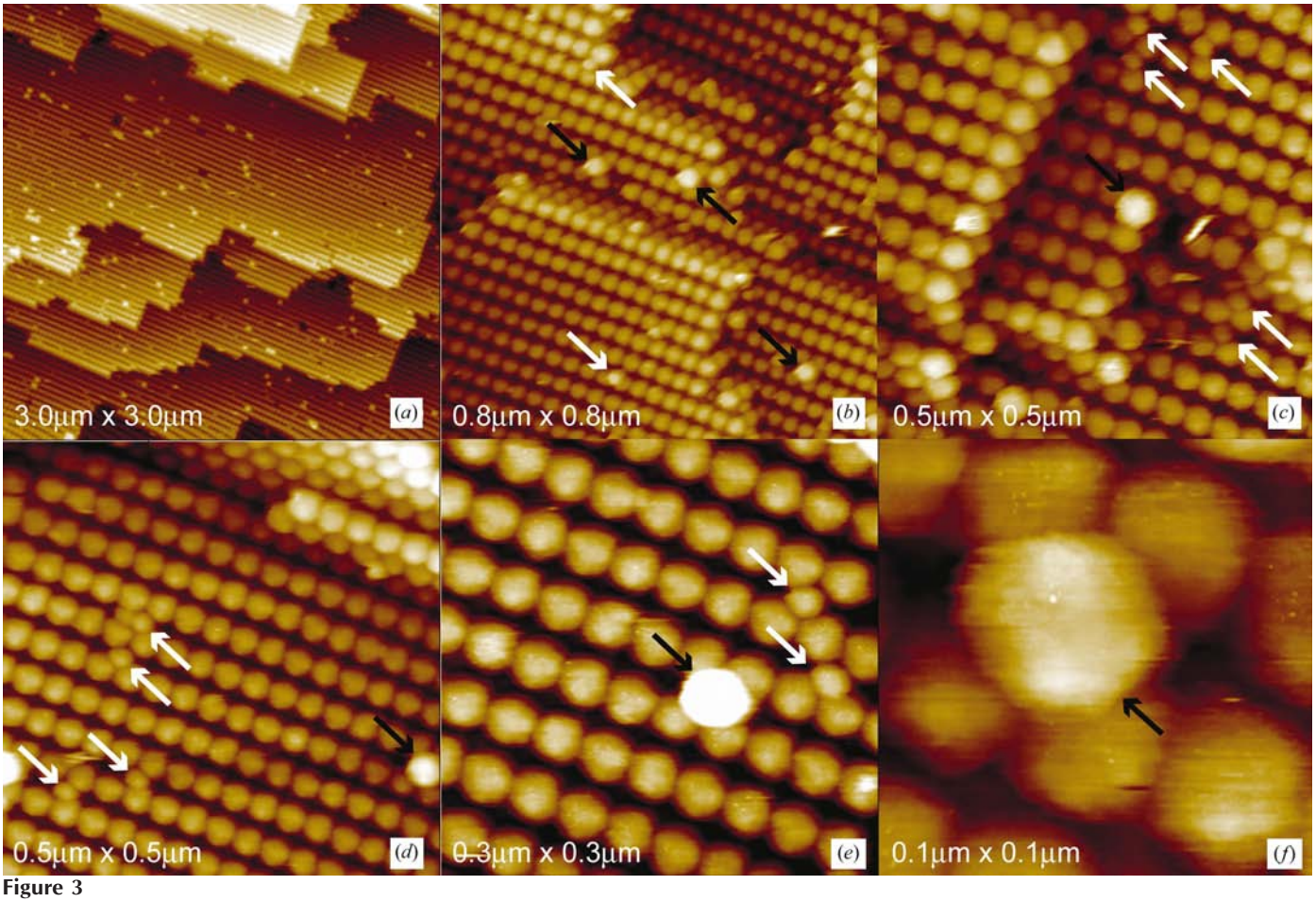

Figure 3
AFM images of the surfaces of glutaraldehyde-treated PMV crystals. Growth steps can be observed in the top row of images. Satellite virus, SPMV, which is indicated by white arrows, can also be seen incorporated between PMV virions in the lattice. Some individual PMV particles, indicated by black arrows, adhere to the surface as well.

grath, 1999). Crystal properties and data statistics are presented in Table 1. For molecular replacement, rotation and translation-function routines from *CNS* v.1.1 (Brünger *et al.*, 1998) were used with data in the range 20–8 Å and a σ cutoff of 2.0.

2.4. Atomic force microscopy (AFM)

Investigation of the surfaces of crystals was carried out using a sealed 75 µl fluid cell as previously described (Kuznetsov *et al.*, 1997; McPherson *et al.*, 2000, 2001). The instrument was a Nanoscope IIIa (Veeco Instruments, Santa Barbara, CA, USA) with oxide-sharpened silicon nitride tips operated in tapping mode. Two problems had to be overcome in order to succeed with AFM imaging. Firstly, scanning was almost impossible in the 30% PEG mother liquor because of its high viscosity. Secondly, crystal surfaces were generally heavily contaminated with amorphous protein precipitate. Most of the crystals, however, had nucleated and grown in contact with the plastic surface of the sitting-drop well. The first problem was therefore solved by prying the crystals from their plastic substrate and turning them over so that their clean underside could be exposed to the AFM tip.

The second problem of the high-viscosity fluid was solved by lightly fixing the crystals with glutaraldehyde before carrying out the AFM analysis in pure water. To avoid disordering the crystals, fixation was carried out by vapor diffusion. This was achieved by adding 6 µl 25% glutaraldehyde to the 0.6 ml reservoir and equilibrating the crystal containing drop for an additional three weeks.

3. Results and discussion

Because of program limitations, the full data set of about 17 million reflections obtained from a single crystal had to be broken up into four different sets and scaled to one another. Statistics for the 2 279 719 independent reflections to 2.7 Å resolution are shown in Table 1. Indexing the structure amplitudes was initially problematic since the unit-cell parameters appeared to be consistent with cubic, tetragonal or orthorhombic unit cells. However, it became apparent from symmetry averaging of reflections, consideration of systematic absences and analysis of simulated precession images using the *HKLVIEW* program from the *CCP*4 suite (Collaborative Computational Project, Number 4, 1994) that the PMV crystals belonged to the monoclinic space group $P2_1$.

There are no corresponding icosahedral and crystallographic symmetry elements possible for space group $P2_1$; hence, the asymmetric unit of the crystals had to be some multiple of a complete virion. Comparing the volume of the $P2_1$ unit cell with the volumes of unit cells from other virus crystals (http://mmtsb.scripps.edu/viper/), we concluded that there were two entire virus particles comprising the asymmetric unit of the crystals. This assumption yields a volume to weight ratio V_M (Matthews, 1968) of 3.66 Å^3 Da^{-1} which, although still high when compared with most protein crystals, is nonetheless consistent with values found for other virus crystals. This presented the problem of deducing the relative dispositions of the two virions comprising the asymmetric unit.

Table 1
Crystal properties and data statistics.

Values in parentheses are for the highest resolution shell.

Wavelength (Å)	1.000
Space group	$P2_1$
Z	4
Unit-cell parameters (Å, °)	a = 411.74, b = 403.90, c = 412.46, β = 89.65
No. observations	17212205
No. unique reflections	2279719
Crystal mosaicity (°)	0.373–0.544
Resolution range (Å)	50.01–2.71 (2.81–2.71)
Completeness (%)	63.0 (4.9)
R_{merge} (%)	13.6 (34.6)
$I/\sigma(I)$	6.8 (2.5)
Redundancy	7.55 (3.14)

The near-equivalence of the three crystallographic axes suggested that the unit cell might be pseudo-cubic or at least that the icosahedral particles might be packed consistent with such symmetry. To further explore this possibility, an AFM investigation of the crystals was undertaken. It was not possible to image the crystals in their mother liquor or under growth conditions, but following mild fixation with glutaraldehyde they could be imaged in fully hydrated form under water.

Fig. 3 contains images of crystal surfaces; the individual virions can be clearly seen as they are arranged in the lattice. Several layers are visualized and step edges are clearly defined. Although the crystal is not actively growing, it is apparent that it develops by the mechanism of two-dimensional nucleation on surfaces. No screw dislocations were observed; indeed, we have yet to observe such dislocations on any virus crystal, although they are common on almost all protein crystals (McPherson *et al.*, 2000, 2001).

Unincorporated PMV virions adhere to the crystal surfaces in most images. In Figs. 3(*e*) and 3(*f*) one such virion lies atop four that are part of the underlying lattice. From this image, we obtain an estimate of the broadening of particles owing to the AFM tip shape and see that it almost doubles the true width of the particle. Its height, however, is consistent with the crystallographic dimensions deduced by X-ray diffraction.

An exceptional observation with these PMV crystals is that they sometimes incorporate virions of the contaminating SPMV (diameter 160 Å) in the PMV crystal lattice between PMV virions occupying legitimate lattice sites. The SPMV, marked by white arrows in Fig. 3, are indeed incorporated into the crystal and are not simply adsorbed to its surface. This is shown by their true lateral dimension in the micrograph. The SPMV particles are lodged in the cavity prepared for the next layer of PMV particles, one of which is indicated by the black arrow. The presence of the SPMV particles precludes the inclusion of PMV particles at these locations without appreciably perturbing the surrounding lattice. We have not previously observed such a phenomenon, although the incorporation of virions of aberrant size into virus crystals at normal lattice positions has been observed (Lucas *et al.*, 2001;

Kuznetsov *et al.*, 2001; Malkin & McPherson, 2002). In those cases, however, defects accompanied their incorporation.

It was not possible in these AFM images to resolve the individual capsomeres on the virion surfaces, although we have often been able to do so on crystals of similar $T = 3$ and even $T = 1$ viruses. This may be a consequence of glutaraldehyde fixation or it may be that the capsomeres are relatively flat and the virion surfaces smooth. In such cases it may be difficult to distinguish topological features. Because capsomeres were not identified, the AFM images provided no information regarding particle orientation in the crystals or relative orientations of the two molecules within the crystallographic asymmetric unit.

For molecular-replacement purposes, a BLAST search (Altschul *et al.*, 1997) with the PMV amino-acid sequence identified tobacco necrosis virus (TNV; Oda *et al.*, 2000) and cocksfoot mottle virus (CfMV; Tars *et al.*, 2003) as having the greatest similarity. Identities of 22.6% in the case of TNV and 26.4% for CfMV were found from a PIR (*SSEARCH* v. 3.0; Smith & Waterman, 1981) alignment with PMV. CfMV, however, belongs to the *Sobemovirus* family, while TNV and PMV both belong to the *Tombusviridae*; hence, TNV was selected as the initial search model.

Using a full TNV particle as probe for molecular replacement (Rossmann, 1990), the rotation and translation functions (*CNS* v. 1.1; Brünger *et al.*, 1998) indicated two discrete but closely related rotation solutions but a single translation solution at ($\sim\frac{1}{4}$, 0, 0). Because of the very large number of atoms involved, it was difficult to search for a translation position of the second particle while fixing the first. It was concluded that the two particles had unique orientations but the position of the second particle was related to the first by a translation of (0, $\frac{1}{2}$, $\frac{1}{2}$), equivalent to a shift of origin in space group $P2_1$. Identical results were obtained using CfMV as the probe. Assuming a twofold relationship between the rotation solutions, a prominent peak might be expected in the Patterson map at (0, $\frac{1}{2}$, $\frac{1}{2}$) arising from the interatomic vectors between particle 1 and particle 2. A native Patterson map calculation using *CNS* with 40–8 Å data was indeed characterized by a strong peak 21.5% the height of the origin peak within 6.3 Å of (0, $\frac{1}{2}$, $\frac{1}{2}$). A second similar peak was also found near ($\frac{1}{2}$, $\frac{1}{2}$, 0), which represents the interatomic vectors between particles related by the 2_1 screw axis.

This conclusion was confirmed by comparing self-rotation function solutions (*GLRF* v. 4.1; Tong & Rossmann, 1990) of the observed data and the self-rotation function using calculated structure factors ($F_{\rm calc}$) of the two particles positioned as

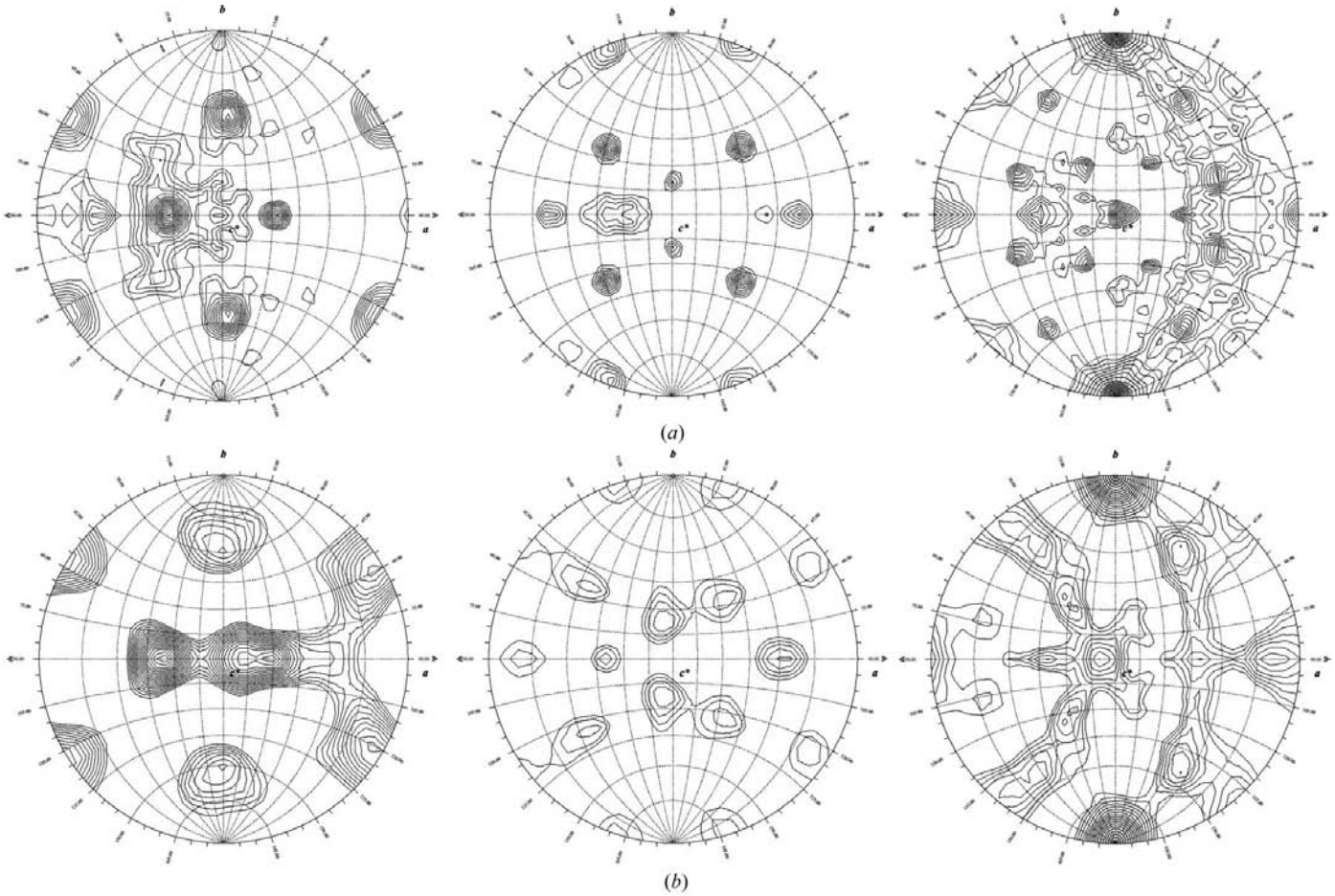

Figure 4
Self-rotation function plots for, from left to right, κ sections 72, 120 and 180°. They were computed using observed data (*a*) and calculated structure factors from the TNV model (*b*), both in the resolution range 40–10 Å.

indicated by the molecular-replacement analysis. The solutions were computed over a series of resolution ranges, with the interval 40–10 Å providing the clearest result. The relevant κ sections are shown in Fig. 4.

The distributions of peaks in Fig. 4 at κ sections 72, 120 and 180° using F_{calc} values closely resembles the self-rotation function solution obtained using F_{obs} and are consistent with the overall icosahedral symmetry of the virus. This further confirms the molecular-replacement solution. In addition, the presence of strong peaks along the x and z axes at $\kappa = 180°$ are consistent with a near but not exact twofold axis of symmetry relating particle 1 to particle 2. For the F_{obs} self-rotation function calculation, the discrepancy between the sets of symmetry elements for the two particles became more significant as the resolution was increased and for rotation functions which included data beyond 5 Å resolution the peaks spread and disappeared into background.

Fig. 5(*a*) shows an arrangement of rows of particles separated by a gap of about 100 Å, which is comparable with the AFM images. When the crystals were imaged by AFM under 80% ethanol instead of water, the particles underneath could clearly be seen between the gaps in the rows of particles, as shown in Fig. 6. The molecular-replacement searches, self-rotation functions and Patterson maps are consistent with one another and indicate that the virus particles are indeed packed in a pseudo-face-centered cubic arrangement. Such a result might have been anticipated from the similarity of the unit-cell parameters. Inspection of the AFM images of the PMV crystals is fully consistent with the face-centered pseudo-cubic lattice arrangement of the particles. As seen in Figs. 3 and 6, successive layers are offset in both directions in the plane by half a particle width, such that every other layer is equivalent in particle positioning.

Interparticle distances were obtained from multiple measurements from three AFM images. Fig. 5(*b*) shows how these distances compare with those predicted from corresponding distances deduced by X-ray diffraction. The variance as well as the percentage difference between the AFM and predicted values are also shown. The measured values indicate that the largest distortion occurs along the scanning direction (horizontal). This may arise from a slight movement or drift of the crystal during imaging. The more precise measurement is the height, which is in exact agreement with the calculated interplanar spacing of the (101) plane based on X-ray results.

4. Conclusion

From these analyses, the orientations of icosahedral symmetry elements for both virions have been found and all NCS operators within the asymmetric unit have been defined. The packing arrangement of the particles within the crystal was predicted from the X-ray diffraction analysis; it correlates well with that deduced from the AFM images.

Currently, we are attempting to refine the position, orientation and diameter of the two particles based on a TNV

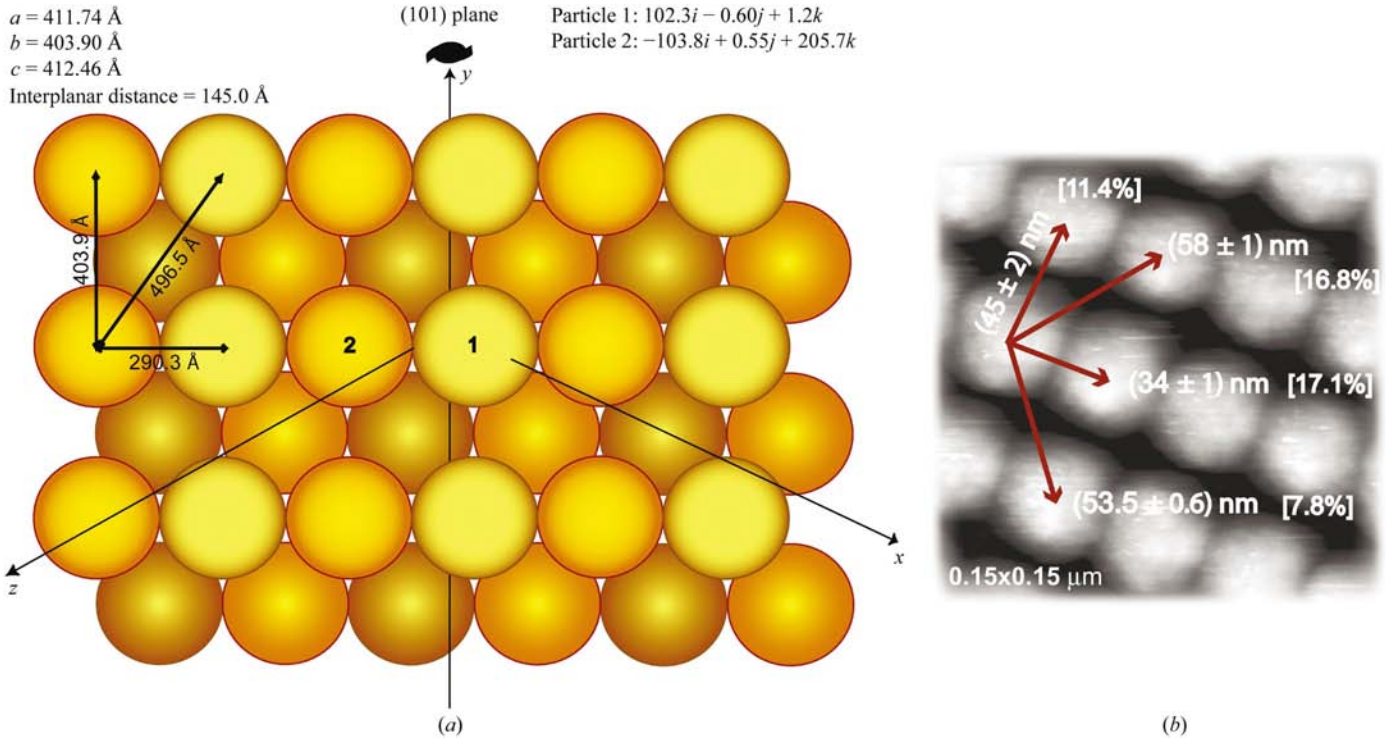

Figure 5
(*a*) Schematic representation of packing of virions in the (101) plane based on crystallographic data. The two different PMV particles in the asymmetric unit are in different colors. Calculations were based on unit-cell parameters and particle-center positions derived from molecular replacement. (*b*) AFM image of a glutaraldehyde-treated PMV crystal. Distances have been derived by averaging over all measurements performed in three different images. Values in square brackets indicate percentage difference from crystallographic values. The interplanar distance is 15 ± 1 nm (3.4%).

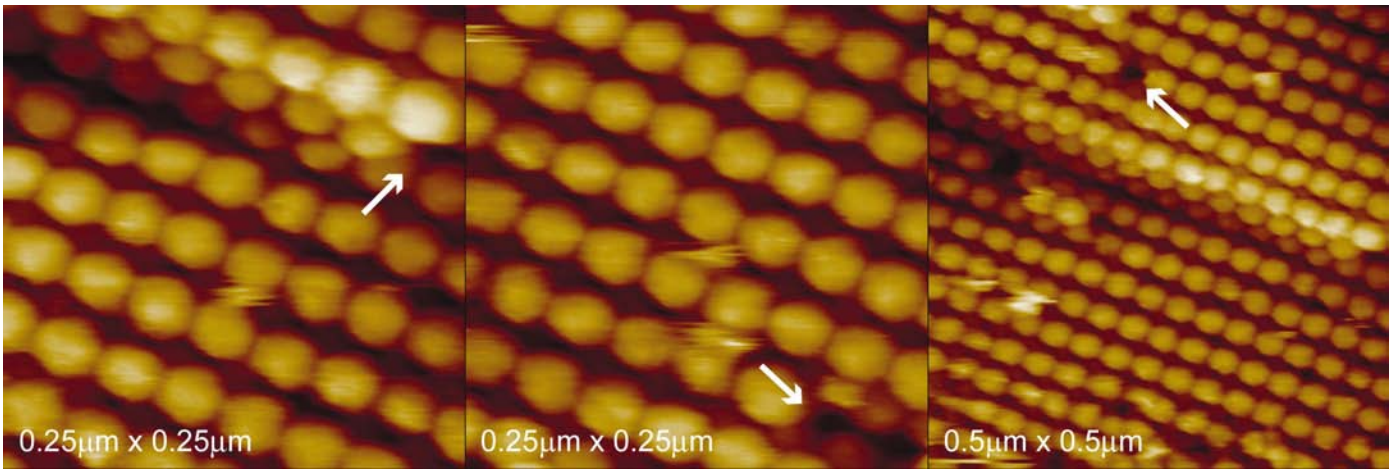

Figure 6
AFM images of the surface of a PMV crystal imaged in 80% ethanol. Missing PMV particles in the top layer, as indicated by arrows, reveals the lattice underneath, which shows the intercalated arrangement of this plane.

starting model in order to obtain accurate NCS operators for phase extension and structure refinement.

We thank Marco Plomp for sharing his technical knowledge regarding AFM imaging, Yu. G. Kuznetsov for his valuable help in obtaining higher quality AFM images and Suliman Rastagar for producing and purifying most of the PMV samples. This work was supported by CNPq (Conselho Nacional de Desenvolvimento Científico e Tecnológico), an entity of the Brazilian government for the development of science and technology, NASA and an NIH grant.

References

Altschul, S. F., Madden, T. L., Schaffer, A. A., Zhang, J., Zhang, Z., Miller, W. & Lipman, D. J. (1997). *Nucleic Acids Res.* **25**, 3389–3402.
Ban, N., Larson, S. B. & McPherson, A. (1995). *Virology*, **214**, 571–583.
Ban, N. & McPherson, A. (1995). *Nature Struct. Biol.* **2**, 882–890.
Brünger, A. T., Adams, P. D., Clore, G. M., DeLano, W. L., Gros, P., Grosse-Kunstleve, R. W., Jiang, J.-S., Kuszewski, J., Nilges, M., Pannu, N. S., Read, R. J., Rice, L. M., Simonson, T. & Warren, G. L. (1998). *Acta Cryst.* D**54**, 905–921.
Buzen, F. G., Niblett, C. L., Hooper, G. R., Hubbard, J. & Newman, M. A. (1984). *Phytopathology*, **74**, 313–318.
Collaborative Computational Project, Number 4 (1994). *Acta Cryst.* D**50**, 760–763.
Kaper, J. M. (1975). *The Chemical Basis of Virus Structure, Dissociation and Reassembly*, edited by A. Neuberger & E. L. Tatum, p. 485. Amsterdam: North-Holland.
Kuznetsov, Y. G., Larson, S. B., Day, J., Greenwood, A. & McPherson, A. (2001). *Virology*, **284**, 223–234.
Kuznetsov, Y. G., Malkin, A. J., Land, T. A., DeYoreo, J. J., Barba, A. P., Konnert, J. & McPherson, A. (1997). *Biophys. J.* **72**, 2357–2364.
Lucas, R. W., Kuznetsov, Y. G., Larson, S. B. & McPherson, A. (2001). *Virology*, **286**, 290–303.
McPherson, A., Malkin, A. J. & Kuznetsov, Y. G. (2000). *Annu. Rev. Biophys. Biomol. Struct.* **29**, 361–410.
McPherson, A., Malkin, A. J., Kuznetsov, Y. G. & Plomp, M. (2001). *Acta Cryst.* D**57**, 1053–1060.
Malkin, A. J. & McPherson, A. (2002). *J. Phys. Chem. B*, **106**, 6718–6722.
Matthews, B. W. (1968). *J. Mol. Biol.* **33**, 491–497.
Oda, Y., Saeki, K., Takahashi, Y., Maeda, T., Naitow, H., Tsukihara, T. & Fukuyama, K. (2000). *J. Mol. Biol.* **300**, 153–169.
Pflugrath, J. W. (1999). *Acta Cryst.* D**55**, 1718–1725.
Rossmann, M. G. (1990). *Acta Cryst.* A**46**, 73–82.
Scholthof, K. B. G. (1999). *Mol. Plant-Microbe Interact.* **12**, 163–166.
Smith, T. F. & Waterman, M. S. (1981). *J. Mol. Biol.* **147**, 195–197.
Tars, K., Zeltins, A. & Liljas, L. (2003). *Virology*, **310**, 287–297.
Tong, L. & Rossmann, M. G. (1990). *Acta Cryst.* A**46**, 783–792.
Turina, M., Maruoka, M., Monis, J., Jackson, A. O. & Scholthof, K. B. G. (1998). *Virology*, **241**, 141–155.
Weiss, M. S. (2001). *J. Appl. Cryst.* **34**, 130–135.